JOURNAL OF PROPULSION AND POWER
Vol. 25, No. 1, January–February 2009

Computational Analyses of Offset-Stream Nozzles for Noise Reduction

Vance Dippold III* and Lancert Foster†
NASA John H. Glenn Research Center at Lewis Field, Cleveland, Ohio 44135
and
Michael Wiese‡
Analytical Services and Materials, Hampton, Virginia 23681

DOI: 10.2514/1.34943

Reynolds-averaged Navier–Stokes calculations were performed on two offset-stream-nozzle concepts for jet noise reduction. The first concept used an S-duct to direct the secondary stream to the lower side of the nozzle. The second concept used vanes to turn the secondary flow downward. The analyses were completed in preparation for a series of experimental tests in which noise and flowfield measurements would be made. The offset-stream nozzles demonstrated good performance and reduced the amount of turbulence on the lower side of the jet plume. The computer analyses proved instrumental in guiding the development of the final test configurations and giving insight into the flow mechanics of offset-stream nozzles. The computational predictions were compared with flowfield results from the jet-rig testing and showed excellent agreement.

Nomenclature

C_d	=	discharge coefficient
C_{fg}	=	thrust coefficient
c	=	vane chord length
D	=	diameter of the secondary-flow nozzle exit
k	=	turbulent kinetic energy
k^*	=	nondimensionalized value of turbulent kinetic energy (k/u_{jet}^2)
M	=	Mach number
$\dot{m}$	=	mass flow rate
p	=	pressure
T	=	temperature
u	=	axial velocity
u_{jet}	=	mass-averaged axial velocity of the primary jet
x, y, z	=	coordinate system
$\Delta(C_dC_{fg})$	=	difference in the thrust parameter of the current configuration from the baseline configuration

Subscripts

LE	=	vane leading edge
peak	=	maximum value in the plume
TE	=	vane trailing edge
0	=	total property
∞	=	freestream property

Introduction

TODAY'S jetliners are significantly more efficient and quieter than commercial jetliners of the 1960s and 1970s. Even so, the goal of reducing noise from aircraft in communities surrounding airports continues to exist. Aircraft manufacturers are increasingly motivated by stringent noise-abatement regulations in airport communities. Traditionally, much of the noise heard during takeoff and landing comes from the aircraft's engines, and much of that noise is jet noise. Jet noise is produced by the shear layers of the jet plume: the core stream, fan stream, and freestream.

Much research has been exerted on jet engine nozzles to hasten the mixing of the shear layers without significantly reducing performance. Papamoschou and Debiasi [1] and Papamoschou [2–4] investigated offsetting the fan stream using fan-flow deflectors: vanes and wedges. Fan-flow deflectors direct the fan stream to the lower side of the jet plume to reduce jet noise observed on the ground by reducing the velocity gradient on the lower side of the jet plume. Papamoschou reported very positive results from his offset-fan-stream experiments. Zaman [5] also investigated offsetting the fan stream using an eccentric nozzle and found favorable noise reduction.

Henderson et al. [6] and Brown and Bridges [7] sought to expand upon these earlier works. Flowfield and acoustical measurements were taken for offset-stream nozzles using S-ducts, vanes, and wedges to direct the fan flow. Higher-bypass-ratio nozzles were used, as that is the direction the industry is headed. Additionally, the tests used larger-scale models and heated-core flows. The work presented in this discussion involves the computational fluid dynamic (CFD) analyses performed on offset-stream nozzles using S-ducts and vanes in preparation for the jet-rig testing. In a companion paper, DeBonis [8] performed CFD analyses on offset-fan-stream nozzles using wedges.

Present Goals

The primary purpose of this set of CFD analyses on offset-stream-nozzle configurations was to prepare for experimental testing in the nozzle acoustic test rig (NATR) at the NASA John H. Glenn Research Center at Lewis Field (GRC). Before manufacturing hardware, it was necessary to verify that the nozzle configurations produced jet flows that were free of significant losses and noise sources, such as shocks or flow separations. An aim of the computational analyses was to screen various vane-nozzle configurations and to help determine which parameters were important for a modern design-of-experiments (MDOE) test matrix (e.g., vane angle of attack and axial and azimuthal locations) so that the proper hardware could be manufactured. Additionally, the CFD solutions predicted the forces produced on the vanes so that they could be manufactured to withstand necessary loads. The CFD solutions also provided details of the nozzle flowfield that could not

Presented as Paper 3589 at the 13th AIAA/CEAS Aeroacoustics Conference, Rome, 21–23 May 2007; received 3 October 2007; revision received 11 April 2008; accepted for publication 21 April 2008.

*Aerospace Engineer, Inlet and Nozzle Branch. Member AIAA.
†Aerospace Engineer, Inlet and Nozzle Branch.
‡Information Technology Specialist.

be easily measured or observed during the NATR testing, such as the internal flow around the vanes.

Modeling

Nozzle Configurations

Two dual-stream subsonic-nozzle models were used for this computational study: the 5BB nozzle from GRC [9] and a nozzle from NASA Langley Research Center (LaRC). Both nozzles were developed to study nozzle flows with a bypass ratio (BPR) of eight. The flow lines for the baseline nozzles are illustrated in Fig. 1. The 5BB nozzle had a fan-stream-nozzle diameter D of 9.63 in., and the LaRC nozzle had a fan-stream-nozzle diameter D of 9.42 in.

Three S-duct configurations were tested. The fan stream was offset from the axis using an S-duct located upstream of the convergent section of the fan-stream nozzle. Previous studies found poor performance when incorporating the S-duct into the convergent portion of the fan-stream nozzle. Two S-duct configurations used the LaRC baseline nozzle, with offsets of 9.3 and 4.6%D. The 9.3%D offset represented the maximum amount that the fan-stream nozzle could be offset; the 4.6%D offset was less aggressive and offset the fan-stream nozzle by about half the maximum. For consistency with the later offset-stream nozzles simulated, one S-duct configuration used the 5BB baseline, with a moderate offset of 4.5%D. These configuration parameters are listed in Table 1 for each S-duct nozzle. Figure 2 shows a rendering of the Sduct-5BB-45 nozzle.

Seven vane configurations were modeled and analyzed: five for takeoff conditions and two for cruise conditions. The vane configurations used the 5BB nozzle as their baseline. The vanes were simple NACA 0012 airfoils [10] with a chord length of 1.32 in. They spanned across the entire width of the fan stream. Each vane configuration had two pairs of vanes in the fan stream, an upper pair and a lower pair, and each vane had three parameters describing its orientation: angle of attack, azimuthal angle (measured from the bottom), and axial position (measured forward of the fan-stream-nozzle exit). Table 2 lists the parameters for each vane case. Figure 3 shows a rendering of the vane E takeoff configuration.

The experimental tests performed in the NATR only used configurations based on the 5BB nozzle at takeoff conditions. Of the 10 offset-stream nozzles using S-ducts and vanes that were analyzed using CFD, only two configurations were tested in the NATR: Sduct-5BB-45 and vane E. The CFD analyses of all 10 configurations enabled comparisons of the performance and flowfield characteristics between the offset-stream nozzles using S-ducts and vanes.

Table 1 S-duct nozzle configurations

Configuration	Baseline	S-duct offset
Sduct-LaRC-93	LaRC BPR8	9.3% D
Sduct-LaRC-46	LaRC BPR8	4.6% D
Sduct-5BB-45	5BB	4.5% D

Flow Conditions

Results for three sets of nozzle conditions are presented: representative takeoff and cruise conditions and an experimental set point. These conditions are listed in Table 3. The major focus of jet noise reduction is to reduce noise at takeoff, as that is when turbofan engines typically produce the most noise because they are operating at their highest power setting and are closest to observers on the ground. The S-duct and vane nozzles were run at simulated cruise conditions to assess the thrust-performance impact at cruise: the longest part of a commercial subsonic mission. Unlike wedge fan-flow deflectors, which can be removed from the fan stream during cruise, the S-duct and vanes are permanent features in the fan stream, though the vanes should be able to rotate to a minimum-drag angle of attack (AOA). Therefore, if offsetting the fan stream with S-ducts or vanes is going to be viable, they must have minimal impact on nozzle thrust performance at cruise. Experimental data were taken at a slightly different freestream Mach number from the representative takeoff condition. The 5BB baseline, Sduct-5BB-45, and vane E nozzles were rerun at this experimental set point to validate the CFD results directly with experimental results.

Nozzle Grids

Multiblock wall-packed grids were created for each nozzle configuration. Symmetry was exploited to reduce the number of grid points and computational requirements. The baseline 5BB nozzle grid was a 2-D axisymmetric grid. The baseline LaRC BPR8 nozzle grid was a 3-D 22.5 deg azimuthal sector. The vane and S-duct nozzle grids were 3-D 180 deg azimuthal sectors. The grids extended roughly 3.3D radially outward from the nozzle centerline and over 40D downstream of the nozzle. Grid structure was kept similar between each of the 5BB nozzle-based grids and between each of the LaRC BPR8 nozzle-based grids, with the only differences being

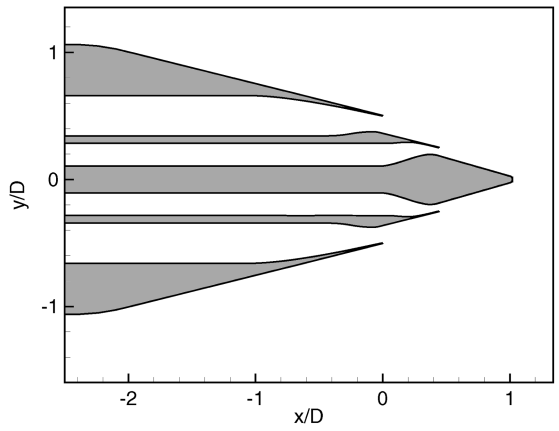

a) LaRC BPR8

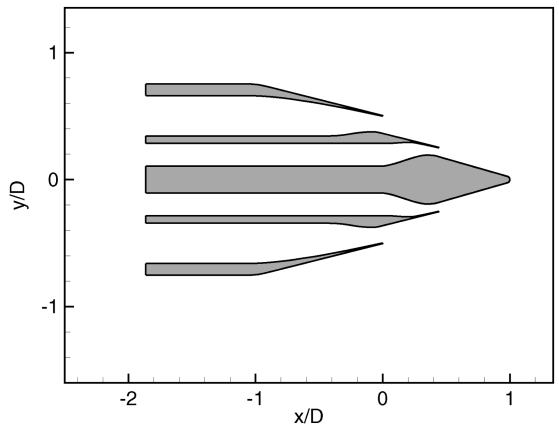

b) 5BB

Fig. 1 Flow lines of baseline nozzles.

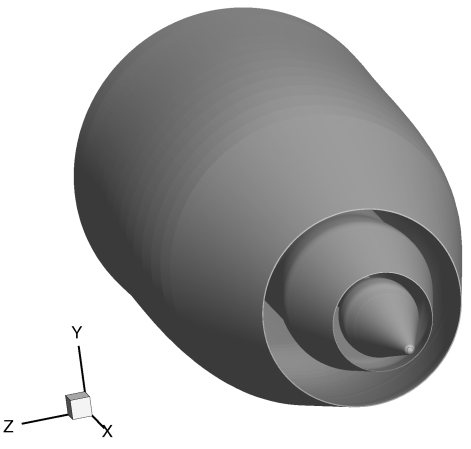

Fig. 2 Rendering of Sduct-5BB-45 offset-stream nozzle.

Table 2 Vane configurations

	Upper vane			Lower vane		
Configuration[a]	AOA, deg	Azimuth,[b] deg	Axial[c]	AOA, deg	Azimuth,[b] deg	Axial[c]
Vane_A	5	130	0 chord	15	50	0 chord
Vane_B	5	130	$\frac{1}{4}$ chord	12	50	$\frac{1}{4}$ chord
Vane_C	5	125	$\frac{1}{4}$ chord	8	55	$\frac{1}{4}$ chord
Vane_D	5	125	$\frac{1}{2}$ chord	12	55	$\frac{1}{2}$ chord
Vane_E	7.5	120	$\frac{1}{2}$ chord	7.5	60	$\frac{1}{2}$ chord
Vane_cruise25	0	125	$\frac{1}{4}$ chord	0	55	$\frac{1}{4}$ chord
Vane_cruise75	0	125	$\frac{3}{4}$ chord	0	55	$\frac{3}{4}$ chord

[a]All vane nozzles use the 5BB baseline.
[b]Azimuthal angle is measured from the bottom of the nozzle.
[c]Axial position is measured as the distance between the vane trailing edge and the fan-stream exit.

where the configuration geometry differed. Figures 4 and 5 show the typical S-duct and vane-nozzle grids; Fig. 6 shows the grid around the vane. The grids consisted of multiple blocks to aid with parallelization on multiprocessor computers to reduce convergence time. The S-duct nozzle grids had about 9 million grid points and the vane-nozzle grids had about 10 million grid points. The 5BB baseline and LaRC BPR8 baseline grids had about 82,000 and 1.5 million grid points, respectively.

Computational Strategy

All of the computational analyses were performed using WIND [11,12] version 5, a general-purpose 3-D Reynolds-averaged Navier–Stokes (RANS) code. WIND is a mature, multizone, structured-grid, compressible flow solver offering a variety of turbulence models. Previous studies [13,14] have shown the Menter shear stress transport (SST) turbulence model [15] to perform superior to WIND's other turbulence models for nozzle flows. Therefore, the SST turbulence model was used for all of the analyses presented in this work.

The size of the nozzle grids required a large amount of computational power to obtain a converged solution. Grid sequencing was used to accelerate solution convergence, beginning with every fourth grid point, then every other grid point, and finally solving with all grid points. Convergence was determined once the change in integrated forces between successive iterations reduced to the order of 0.01%. The typical solution took 5–10 days to adequately converge.

Results

Computational analyses were performed for the S-duct and vane offset-stream nozzles using the WIND code. These analyses supported the design and screening phases of hardware for experimental testing and were iterative in nature. The screening allowed nozzle configurations to be developed that were free from excessive noise sources and thrust losses. For the offset-stream nozzles using vanes, in particular, the final configuration would be the center of a MDOE test matrix, in which it was desired that all configurations would give useful results.

Table 3 Nozzle flow conditions

	Takeoff	Cruise	Experiment
Core stream			
T_0, °R	1498	1421	1498
p_0/p_∞	1.42	2.19	1.42
Fan stream			
T_0, °R	640	509	640
p_0/p_∞	1.62	2.56	1.62
M_∞	0.28	0.8	0.20
Freestream			
p_∞, lb/in.^{2}	14.4	3.46	14.4
T_∞, °R	529.67	394	529.67

In the discussion of the CFD results, contour plots are presented of the axial velocity u normalized by the core-stream velocity mass-averaged at the nozzle exit, u_{jet}, along the jet-plume symmetry plane and at axial cross sections through the plume. Similarly, contour plots of the turbulence parameter k^*, defined by

$$k^* = \frac{k}{u_{\text{jet}}^2} \tag{1}$$

are also presented along the jet-plume symmetry plane and at axial cross sections through the plume. It is helpful to look at turbulent kinetic energy k, because it is directly related to the production of jet noise. The maximum value of the turbulence parameter, k^*_{peak}, was found along azimuthal planes in the jet plume. The length of the primary jet potential core is useful to report. The potential core is defined as

$$u \geq 0.99 \cdot u_{\text{jet}} \tag{2}$$

The nozzle thrust and mass flow were computed using the WIND utility `cfpost` to integrate the mass flow and momentum forces at the nozzle-exit planes and the pressure and viscous forces along the nozzle plug and splitter surfaces. The total thrust in the axial direction

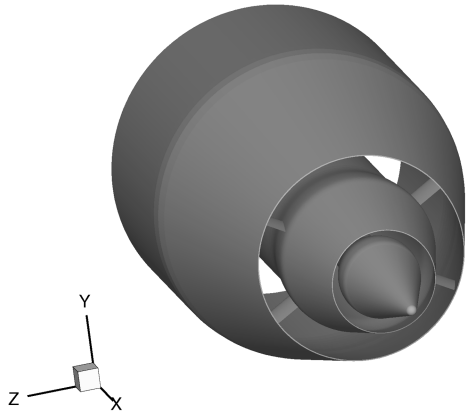

Fig. 3 Rendering of vane_E offset-stream nozzle.

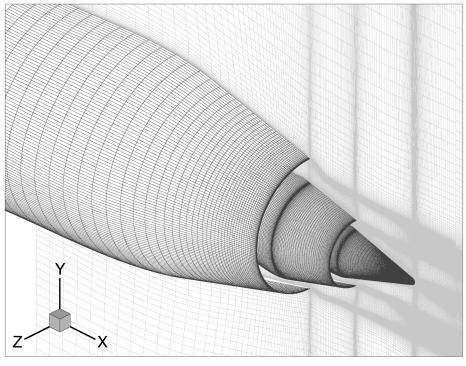

Fig. 4 Grid around Sduct-5BB-45 offset-stream nozzle.

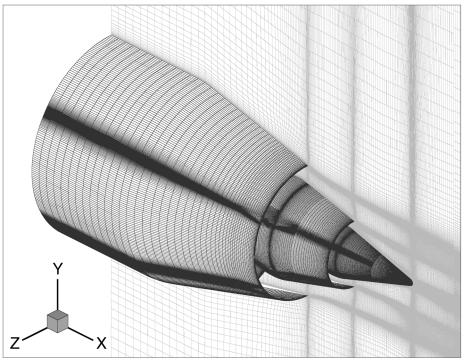

Fig. 5 Grid around vane_E offset-stream nozzle.

was represented as the gross thrust coefficient:

$$C_{fg} = \frac{F_{\text{actual}}}{\dot{m}_{\text{actual}} \cdot U_{\text{ideal}}} \tag{3}$$

The change in mass flow as compared with the baseline nozzle was specified using the discharge coefficient:

$$C_d = \frac{\dot{m}_{\text{actual}}}{\dot{m}_{\text{ideal}}} \tag{4}$$

For subsonic dual-stream nozzles, the over- or underexpansion of one stream can affect the nozzle flow rate of the other stream. The variation in mass flow will result in a thrust coefficient that is not a true representation of the actual performance of the nozzle. To use a thrust coefficient that does give a true measure of the nozzle's performance, the thrust coefficient was then based on the ideal mass flow rather than the actual mass flow, which is simply the product of the discharge coefficient and the thrust coefficient:

$$\frac{F_{\text{actual}}}{\dot{m}_{\text{ideal}} \cdot U_{\text{ideal}}} = \frac{\dot{m}_{\text{actual}}}{\dot{m}_{\text{ideal}}} \cdot \frac{F_{\text{actual}}}{\dot{m}_{\text{actual}} \cdot U_{\text{ideal}}} = C_d \cdot C_{fg} \tag{5}$$

The performance of each offset-stream nozzle was compared with its respective baseline nozzle. To compare the performance of offset-stream nozzles that had different baseline nozzles, the performance of each offset-stream nozzle was referenced to its associated baseline nozzle and reported as $\Delta(C_d C_{fg})$:

$$\Delta(C_d \cdot C_{fg}) = (C_d \cdot C_{fg})_{\text{offset stream}} - (C_d \cdot C_{fg})_{\text{baseline}} \tag{6}$$

Additionally, the thrust-vector angle from the nozzle axis is also reported.

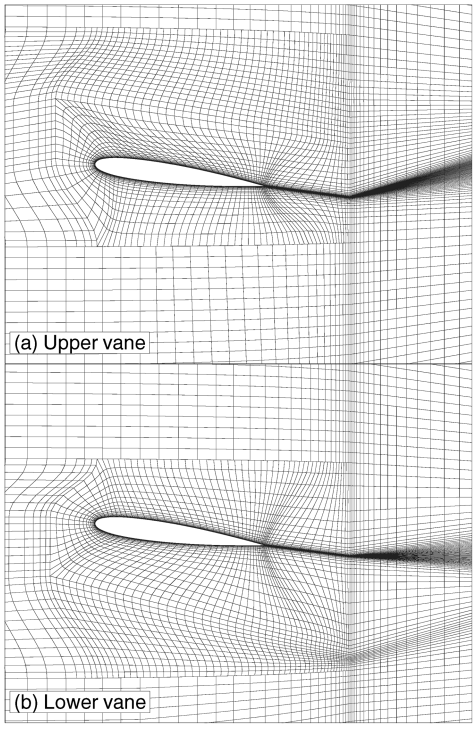

Fig. 6 Grid around vanes of vane_E offset-stream nozzle.

S-Duct Offset-Stream Nozzles

Takeoff Flow Conditions

Two S-duct nozzles based on the LaRC BPR8 nozzle were run at takeoff conditions: the Sduct-LaRC-93 configuration with an aggressive fan-stream offset of 9.3%D and the Sduct-LaRC-46 configuration with a moderate fan-stream offset of 4.6%D. The velocity contours along the symmetry plane are compared with the LaRC BPR8 baseline nozzle in Fig. 7. The S-duct nozzles are shown to redirect the fan-stream flow to the lower side of the nozzle. The length of the core-stream potential core is plotted in Fig. 8. The Sduct-LaRC-93 nozzle reduces the length of the potential core by over 6.5D, and the Sduct-LaRC-46 nozzle reduces the potential core by nearly 4.5D.

Contours of k^* are plotted in Fig. 9 for the LaRC-based S-duct nozzles. By offsetting the fan stream, the two S-duct nozzles successfully reduce the amount of turbulence on the lower side of the jet plume. This is directly a result of reducing the velocity gradient radially across the jet plume on the lower side of the plume by directing the fan stream. Conversely, because there is less fan flow on the top side of the jet plume, peak values of turbulence increase greatly on the upper side of the plume. On both sides of the jet plume, the region of peak turbulent kinetic energy is moved upstream, as compared with the baseline.

Figures 10a and 10b show the peak values of k^* for the lower and upper portions of the jet plume, and it is observed that the peak values of turbulence increase much more on the upper side of the plume than they decrease on the lower side of the plume. As expected, the moderately offset Sduct-LaRC-46 nozzle has a lower value of peak turbulence on the upper side of the plume than the Sduct-LaRC-93 nozzle. Surprisingly, however, the Sduct-LaRC-46 nozzle also has a significantly lower value of peak turbulence on the lower side of the plume. Figure 10c shows peak values of k^* at the 60 deg azimuthal angle, which should be an indicator of sideline noise. Along this azimuthal plane, the peak value of k^* for the Sduct-LaRC-46 nozzle is less than that of the baseline nozzle. However, the peak value of k^* for the Sduct-LaRC-93 nozzle is significantly larger than that of the baseline nozzle (closer to the peak value of k^* on the upper portion of the plume).

The structure of the jet plume of the S-duct nozzles is observed in Fig. 11, in which turbulent kinetic energy is plotted at different axial cross sections along the plume. At the maximum offset, the Sduct-LaRC-93 nozzle is characterized with a jet plume that is full and round on the lower side. The upper side of the plume is narrow but has a horseshoe-shaped region of strong turbulent kinetic energy from 0.5 to 5.0D downstream of the fan-stream exit. This is due to the large axial velocity gradient between the core stream and the freestream, with very little fan-stream flow between. The plume of the Sduct-LaRC-46 nozzle shows evidence of a similar structure, though with less pronounced features.

Using the results from the CFD analyses, the nozzles' thrust efficiencies were computed. This was important because force measurements were not possible in the NATR during the experimental tests. For each offset-stream nozzle, $\Delta(C_d C_{fg})$ is plotted in Fig. 12, with $\Delta(C_d C_{fg}) = 0$ being equal to the thrust parameter of the associated baseline. Both LaRC BPR8-based S-duct nozzles had a mass-corrected thrust loss of less than 1%, with the aggressively offset Sduct-LaRC-93 nozzle having a 0.2% lower thrust coefficient than the moderately offset Sduct-LaRC-46 nozzle. The thrust angle was also calculated and is plotted in Fig. 13. As expected, offsetting the fan stream to the lower side of the nozzle redirects the thrust vector.

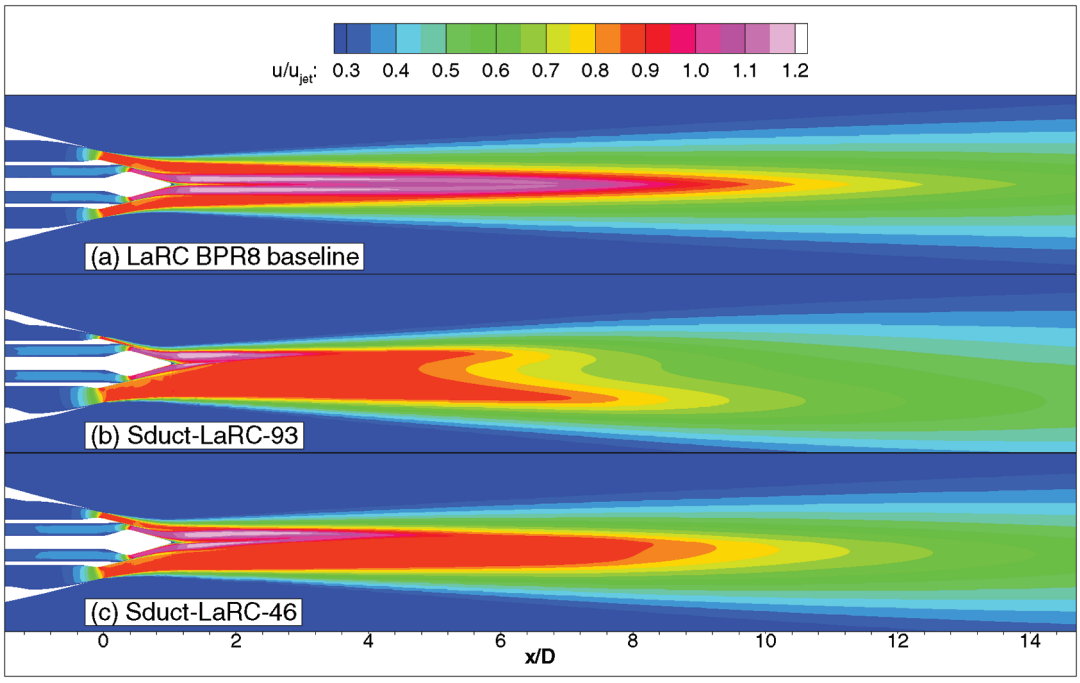

Fig. 7 Velocity contours on symmetry plane of S-duct nozzles and baselines at takeoff flow conditions.

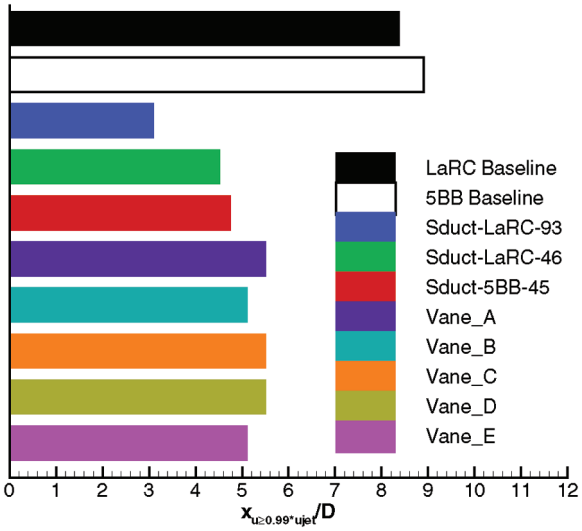

Fig. 8 Length of primary jet potential core for baseline and offset-stream nozzles at takeoff condition.

The moderately offset Sduct-LaRC-46 nozzle had more favorable thrust performance and turbulent-kinetic-energy reduction than the Sduct-LaRC-93 nozzle. The nozzle designed for testing on the NATR, the Sduct-5BB-45 nozzle, used a fan-stream offset similar to the Sduct-LaRC-46 nozzle. The Sduct-5BB-45 nozzle performed similarly to the Sduct-LaRC-46 nozzle. Peak levels of turbulence are shown in Fig. 10. The thrust coefficient is compared with the earlier S-duct nozzles in Fig. 12, and the thrust angle is plotted in Fig. 13.

Cruise Flow Conditions

The S-duct nozzles were also run at cruise conditions. It is generally known that airframe manufacturers will typically refuse any change if the overall performance of the aircraft is reduced more than 0.25%, regardless of the perceived benefit the change brings. Because the vast majority of an aircraft's flight is at cruise conditions, it would be difficult to justify a noise-reduction technique that reduces cruise performance beyond 0.25%.

Velocity contours of the Sduct-LaRC-93 and Sduct-LaRC-46 nozzles are compared with the baseline LaRC BPR8 nozzle in Fig. 14. No unexpected separations or strong shocks were evident. The thrust parameter $\Delta(C_d C_{fg})$ is plotted in Fig. 15. The Sduct-LaRC-46 nozzle had a thrust reduction of less than 0.1% as compared with the baseline nozzle. The more aggressively offset Sduct-LaRC-93 nozzle had a much larger reduction in thrust from the baseline: nearly 0.7%, which was well beyond the acceptable loss of 0.25%. As at takeoff conditions, the Sduct-5BB-45 nozzle performed similarly to the Sduct-LaRC-46 nozzle.

Vane Offset-Stream Nozzles

Computational analyses were completed for offset-stream-nozzle configurations using vanes to turn the fan flow downward. By the time the vane nozzles were being developed, the offset-stream-technology group had decided to use the 5BB nozzle as the bypass-ratio-eight baseline nozzle. As mentioned previously, CFD analyses were performed on seven different vane-nozzle configurations: five takeoff configurations with the vanes angled to direct the fan flow downward to produce the offset-stream effect and two cruise configurations with the vanes angled parallel to the axis to reduce performance losses at cruise conditions.

Takeoff Flow Conditions

Similar analyses were performed at takeoff conditions for five offset-stream nozzles using vanes. The first vane-nozzle configuration, vane_A, placed the lower pair of vanes at an aggressive 15 deg AOA. As will be discussed, later vane-nozzle configurations reduced the lower-vane angle of attack. Additionally, whereas the trailing edge of the vane_A nozzle vanes was located at the fan-stream exit, later configurations moved the vanes upstream, by as much as 50% of the vane chord length. The full details of each vane-nozzle configuration are given in Table 2.

Contour plots of axial velocity along the symmetry plane are compared for the baseline 5BB nozzle and several vane nozzles in Fig. 16. As with the S-duct nozzles, the vane nozzles successfully directed the secondary stream downward. In general, the larger the vane angle of attack, the more the vane nozzle turned the fan stream downward. The potential-core length for each nozzle is plotted in Fig. 8. The vane nozzles reduced the length of the potential core from 8.9 to 5–5.5D downstream of the fan-stream exit. The vane nozzles did not have the same degree of variation in potential-core length as did the S-duct nozzles. Furthermore, the vane nozzles produced a

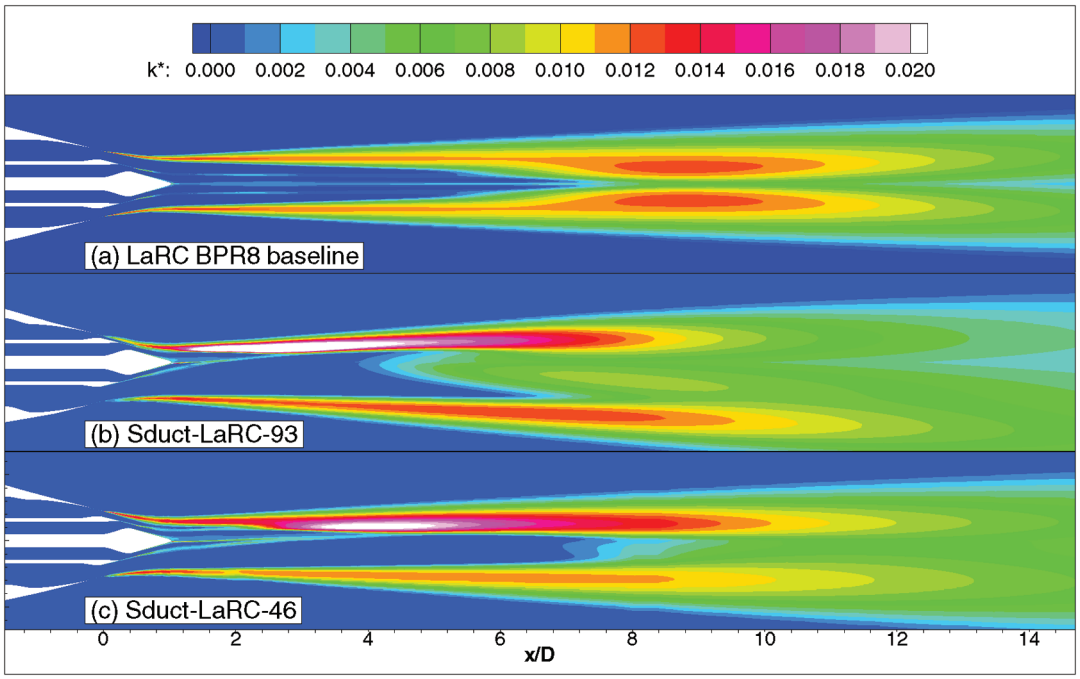

Fig. 9 Turbulence contours on symmetry plane of S-duct nozzles and baselines at takeoff flow conditions.

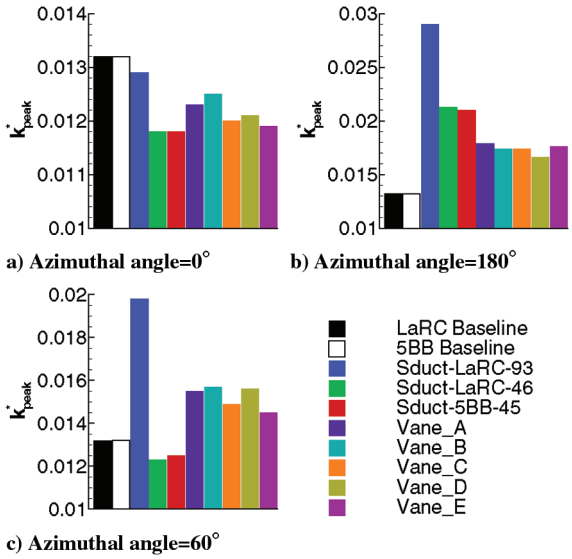

Fig. 10 Peak values of turbulent kinetic energy in the plume at various nozzle azimuth positions. Nozzle bottom, 0 deg; nozzle top, 180 deg; sideline, 60 deg.

potential core that was 0.5–1.0D longer than the moderately offset S-duct nozzles.

Turbulence contours are plotted along the symmetry plane in Fig. 17. Compared with the baseline 5BB nozzle, the vane offset-stream nozzles reduced the turbulent kinetic energy on the lower side of the jet plume and moved the peak turbulence region on the upper side of the plume upstream. The peak values of k^* are plotted in Fig. 10. The more moderate vane-angle configurations (vane_C and vane_E) reduced the peak turbulence on the lower side more than the configurations with larger vane angles, to levels comparable with the moderately offset S-duct nozzles. On the upper side of the plume, the vane nozzles did not increase the peak turbulence nearly as much as observed for the S-duct nozzles. Along the 60 deg azimuthal angle, all of the vane nozzles have peak values of k^* greater than that of the baseline 5BB nozzle, indicating that they may increase sideline noise. These observations suggest that the vane nozzles did not redirect as much flow from the upper side of the fan stream as did the S-duct nozzles.

Contour plots of the turbulent kinetic energy along axial cross sections of the plume are plotted in Fig. 18 for several vane nozzles. Similar to the S-duct nozzles, the vane nozzles also had a horseshoe-shaped region of high turbulence, though the peak was further downstream. The structure of the jet plume in these plots confirms that the vane nozzles did not move as much fan stream from the top to the bottom of the nozzle as did the S-duct nozzles. In contrast to the S-duct nozzle plumes (Fig. 11), the plume of the vane nozzles were full and round on the upper side and thin on the lower side. Furthermore, the aggressive 15-deg-AOA vanes of the vane_A nozzle and the 12-deg-AOA vanes of the vane_B nozzle pushed the lower portion of the fan stream further downward than the S-duct nozzles. The vanes also gave the jet-plume corners at the vane azimuth locations. Two spots of turbulence were observed inside the lower portion of the fan stream for the vane_A nozzle. This turbulence was thought to be a result of separated flow off the lower pair of vanes, angled at 15 deg.

Another benefit of the WIND CFD solutions was that they allowed the flowfield around the vanes to be observed with ease. Because this portion of the nozzle flow is interior to the nozzle, the flowfield would not be easily observable using experimental techniques. Contours of the Mach number around the lower vanes are plotted in Fig. 19. This plot confirms that separation occurred over a large portion of the 15-deg-AOA vanes of the vane_A nozzle. Furthermore, it shows separated flow near the trailing edge of the 12-deg-AOA vanes of the vane_B nozzle. Although the CFD results did not show that separation over the vanes will increase the noise, as will be revealed shortly, the CFD solutions did show that separated flow reduced the nozzle's mass flow and thrust. In addition to confirming separated flow, Figs. 19a and 19b show that supersonic flow exists on the upper surface of the vane_A and vane_B lower vanes. Although no shocks appear to be present, there exists the possibility that some change in condition or some other small perturbation could produce shocks, leading to increased separation and even increased noise.

Two different methods to reduce the amount of supersonic flow and separated flow over the vanes were attempted. First, the vane angle of attack was reduced. The lower vanes of the vane_B nozzle and the vane_C nozzle had the same axial position, but the vane_C lower vanes had a vane angle of 8 deg, whereas the vane_B lower vanes had an angle of 12 deg. Comparing Figs. 19b and 19c, it is observed that reducing the vane angle of attack did significantly

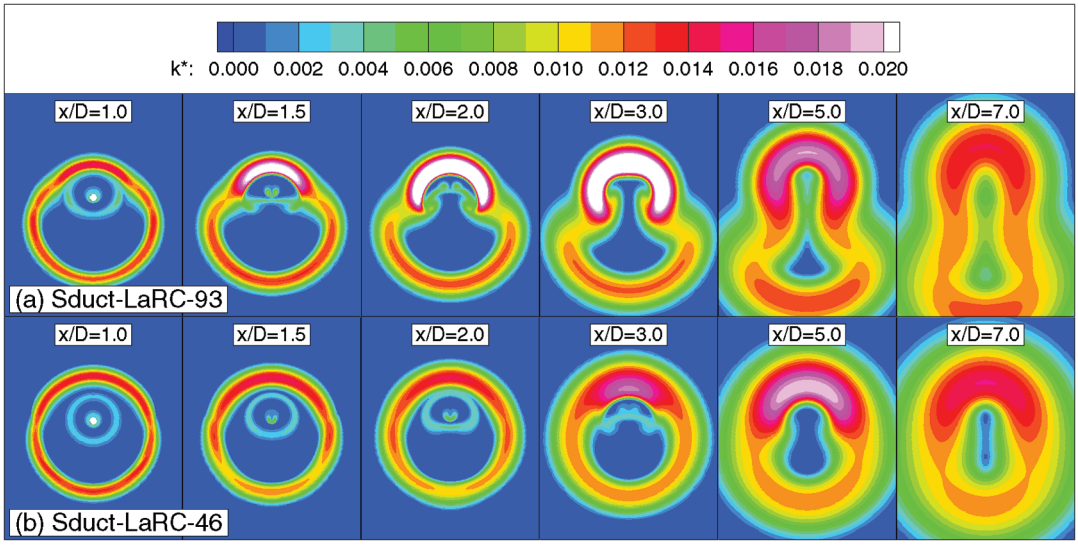

Fig. 11 Turbulence contours at plume cross sections of S-duct nozzles and baselines at takeoff flow conditions.

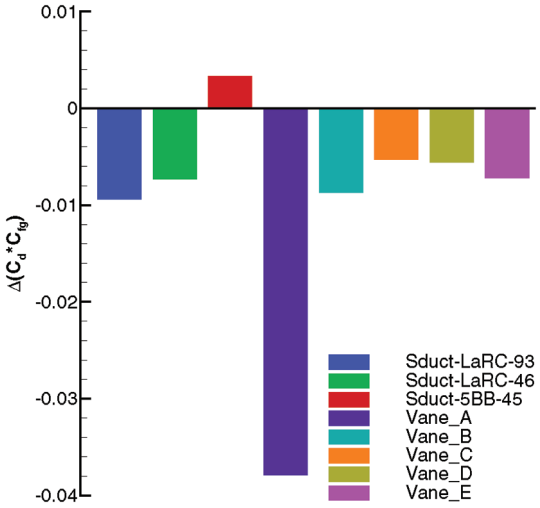

Fig. 12 Thrust performance of offset-stream nozzles at takeoff flow conditions.

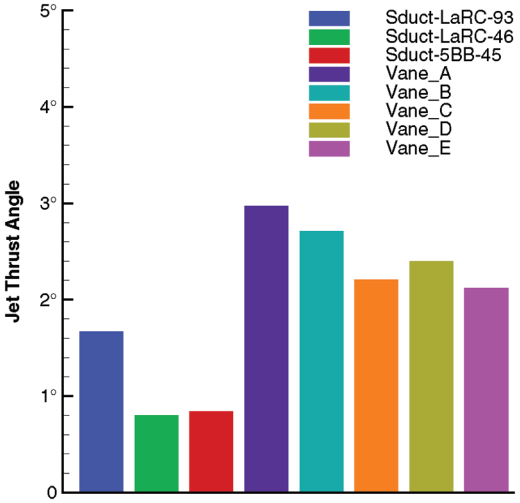

Fig. 13 Thrust angle of offset-stream nozzles at takeoff flow conditions.

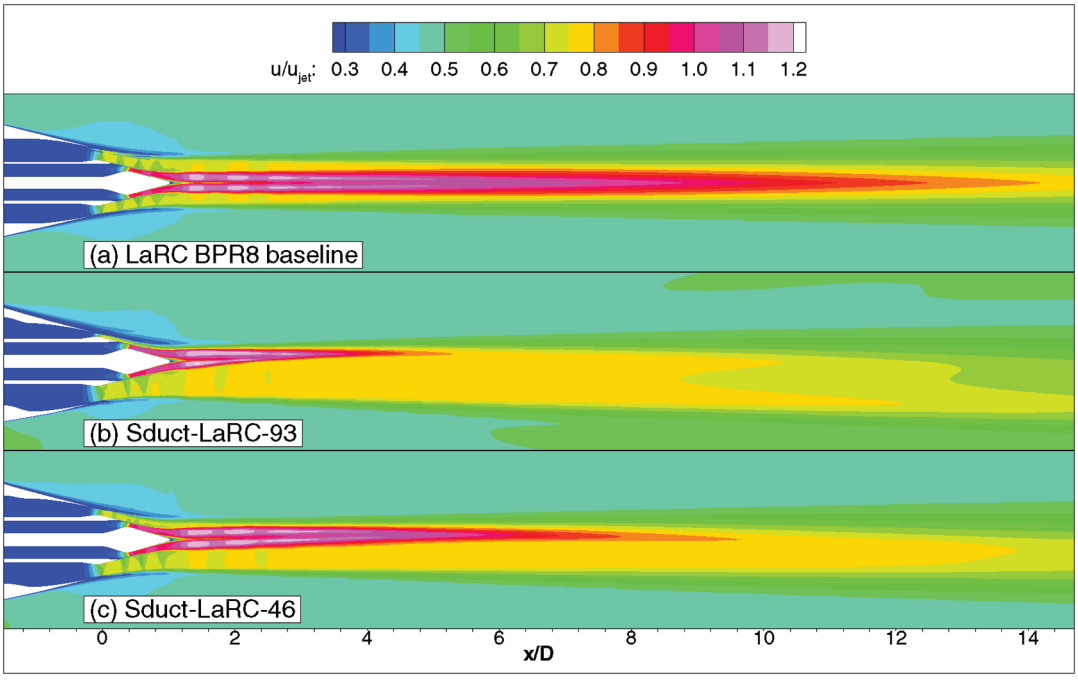

Fig. 14 Velocity contours on symmetry plane of S-duct nozzles and baselines at cruise flow conditions.

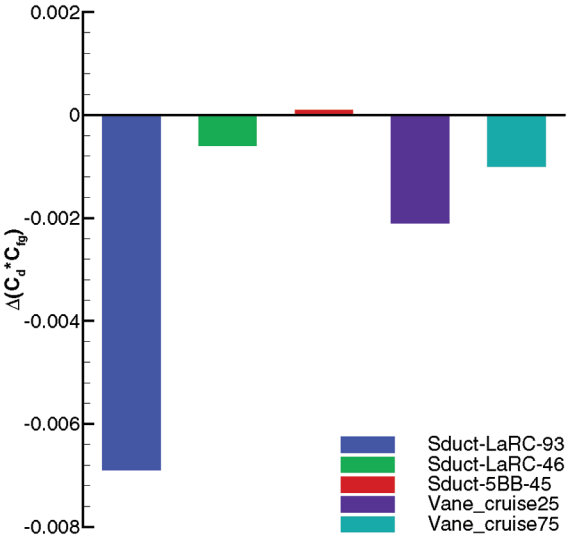

Fig. 15 Thrust performance of offset-stream nozzles at cruise flow conditions.

reduce the size of the region of supersonic flow and reduce the boundary-layer thickness on the upper surface of the vanes.

The second method to reduce the amount of supersonic flow and separated flow over the vanes was to move the vanes farther upstream. The fan-stream nozzle is convergent and the vanes were located in the convergent section of the nozzle, where the flow is accelerating. By moving the vanes farther upstream in the fan-stream nozzle, they would see flow that had not accelerated as much. Table 4 lists the nominal Mach number M in the baseline 5BB nozzle at the leading-edge and trailing-edge locations for each axial vane position $(x/c)_{\mathrm{TE}}$. In Figs. 19b and 19d, the lower vanes of the vane_B nozzle and the vane_D nozzle had the same angle of attack, 12 deg, but the vane_D vanes were positioned a quarter-chord farther upstream than those of the vane_B nozzle. The baseline nozzle Mach number would decrease about 8% at the leading edge and about 10% at the trailing edge by moving the vane a quarter-chord upstream. The result, as observed in Figs. 19b and 19d, was that the region of supersonic flow over the vanes was significantly reduced in size, though not as much so as reducing the vane angle.

The thrust coefficient at the takeoff condition is plotted for each vane nozzle in Fig. 12. The vane_A nozzle is immediately noticed for its 3.8% reduction in $C_d C_{fg}$ from the baseline; the other vane nozzles exhibit losses in the thrust parameter of less than 0.9%. This was a consequence of the large region of separated flow on the lower 15-deg-AOA vanes. Reducing the vane angle to 12 deg on the vane_B nozzle improved the thrust losses. Further reducing the vane angle on the vane_C nozzle and moving the vanes upstream on the vane_D nozzle allowed more improvements in the thrust loss. The vane_B through vane_E nozzles show thrust losses comparable with the S-duct nozzles. The thrust-vector angle is shown for the vane nozzles in Fig. 13. The thrust-vector angle ranges from 2 deg for the vane_E nozzle to 3 deg for the vane_A nozzle (significantly greater than that of the S-duct nozzles).

There were three parameters for each pair of vanes: angle of attack, axial location, and azimuthal angle. The five offset-stream vane nozzles changed two, and sometimes all three, parameters between each iteration of nozzle design. Therefore, no conclusions about the effects of each parameter could be drawn directly. However, based upon the CFD analyses, it can be concluded that angle of attack has a large effect. The axial location of the vane also appears to have an effect, though smaller. It was inconclusive what effect was caused by the vane azimuthal angle. As mentioned previously, jet-rig testing was performed on a number of vane-nozzle configurations in the NASA GRC NATR to better define the effects of the vanes, especially on the jet noise. The various configurations that were tested were determined through MDOE. The vane_E nozzle configuration, although not the best-performing of the vane nozzles, did perform well enough and was representative of the vane nozzles enough that it was used as the center point of the MDOE matrix of configurations. For more information regarding the MDOE matrix developed for the offset-stream-technologies task experiments, the

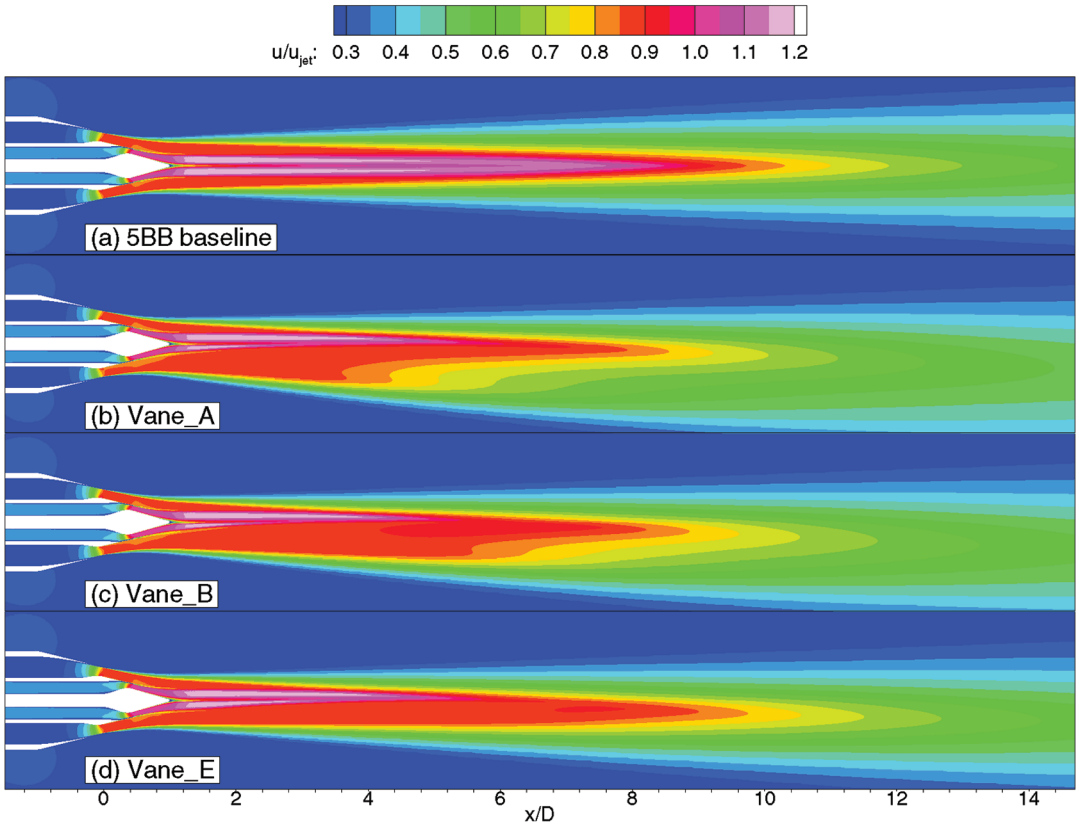

Fig. 16 Velocity contours along symmetry plane of vane offset-stream nozzles at takeoff flow conditions.

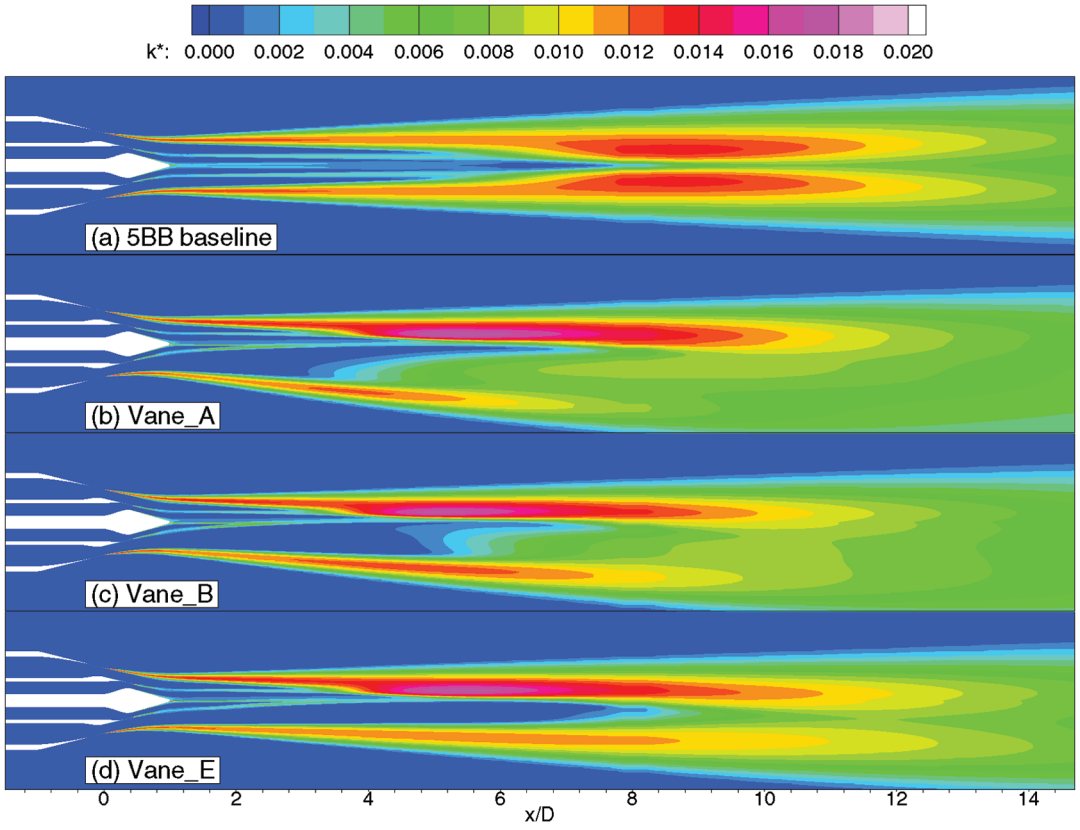

Fig. 17 Turbulence contours along symmetry plane of vane offset-stream nozzles at takeoff flow conditions.

reader is invited to read discussions by Henderson et al. [6] and Brown and Bridges [7].

Cruise Flow Conditions

As with the S-duct nozzles, CFD analyses were run for the vane nozzles at cruise conditions. One advantage that the vane offset-stream-nozzle concept has over the S-duct nozzle concept is that the vanes can be rotated to a minimum-drag position once the aircraft reaches its cruising altitude. (For the NACA 0012 airfoil, this corresponded to a 0 deg AOA.) This is because the noise reduction from offsetting the fan stream is only necessary during takeoff and climb. Two vane-nozzle cruise configurations were modeled and tested: the vane_cruise25 nozzle had the vanes positioned

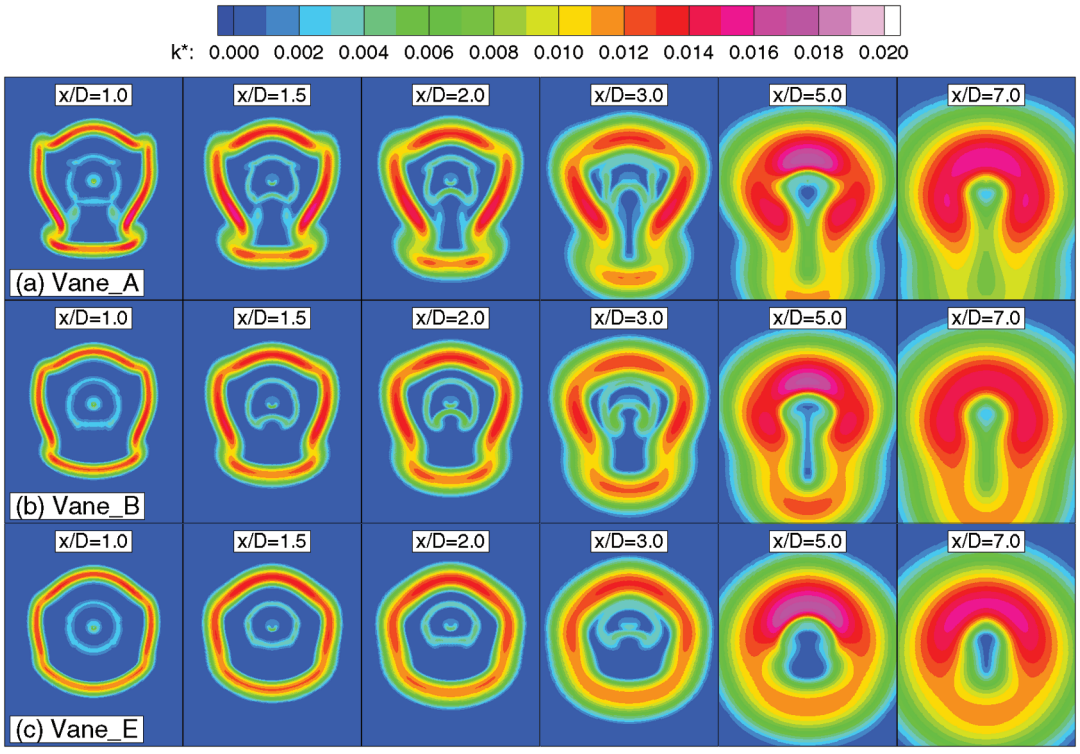

Fig. 18 Turbulence contours at plume cross sections of vane offset-stream nozzles at takeoff flow conditions.

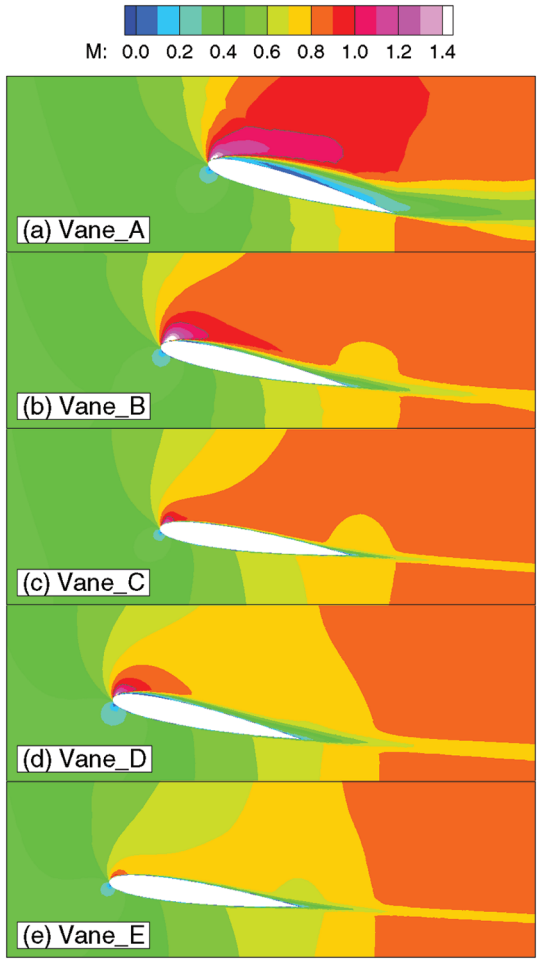

Fig. 19 Mach number contours at midspan of lower vane for vane offset-stream nozzles at takeoff flow conditions.

one-quarter (25%) chord upstream of the fan nozzle exit, and the vane_cruise75 nozzle had the vanes positioned three-quarter (75%) chord upstream of the fan nozzle exit. Figure 20 shows plots of the velocity contours for the vane-nozzle cruise configurations along the symmetry plane. The plumes of the two cruise vane nozzles look nearly identical to the baseline 5BB nozzle at cruise. It appears that the vanes have minimal impact at a 0 deg angle of attack. Figure 21 shows that the flowfield around the vanes is free from separations, shocks, and supersonic regions of flow. Table 5 lists the local Mach number in the baseline 5BB nozzle at the leading-edge and trailing-edge locations for each axial vane position.

Table 4 Mach number at vane leading-edge and training-edge locations in the baseline 5BB nozzle at takeoff conditions

$(x/c)_{TE}$	M_{LE}	M_{TE}
0	0.54	0.84
$-\frac{1}{4}$	0.51	0.79
$-\frac{1}{2}$	0.47	0.71

The thrust parameter $\Delta(C_d C_{fg})$ is plotted for the cruise condition in Fig. 15. At cruise, with the vanes rotated to a 0 deg AOA, the thrust parameter was reduced by about 0.2%, with the vane positioned at one-quarter chord and 0.1% with the vanes positioned at three-quarter chord. These losses are a result of reduced mass flow due to the blockage caused by the vanes in the fan-stream nozzle. The vane_cruise75 nozzle demonstrates that moving the vanes upstream in the convergent fan-stream nozzle reduces the thrust loss, because the nozzle area is greater in the upstream position (whereas the cross-sectional area of the vanes remained constant).

Comparison with Experimental Data

The CFD analyses helped in the development of jet-rig hardware by indicating which vane-nozzle parameters were most important. Even though the WIND code has been validated for jet flows and shown to perform well when predicting the general flowfield, it was still of interest to compare the CFD predictions with experimental data. The experimental flowfield measurements were acquired for the 5BB baseline, Sduct-5BB-45, and vane_E nozzles at $M_\infty = 0.20$, rather than at $M_\infty = 0.28$, which was used during the screening CFD solutions. Therefore, one more CFD analysis was performed for each of these nozzle configurations, adjusting the freestream inflow parameters to correspond to $M_\infty = 0.20$.

Contours of velocity for the CFD solutions and experimental particle image velocimetry (PIV) data are compared in Figs. 22–24. It should be noted that the plots of PIV data do not include data of poor

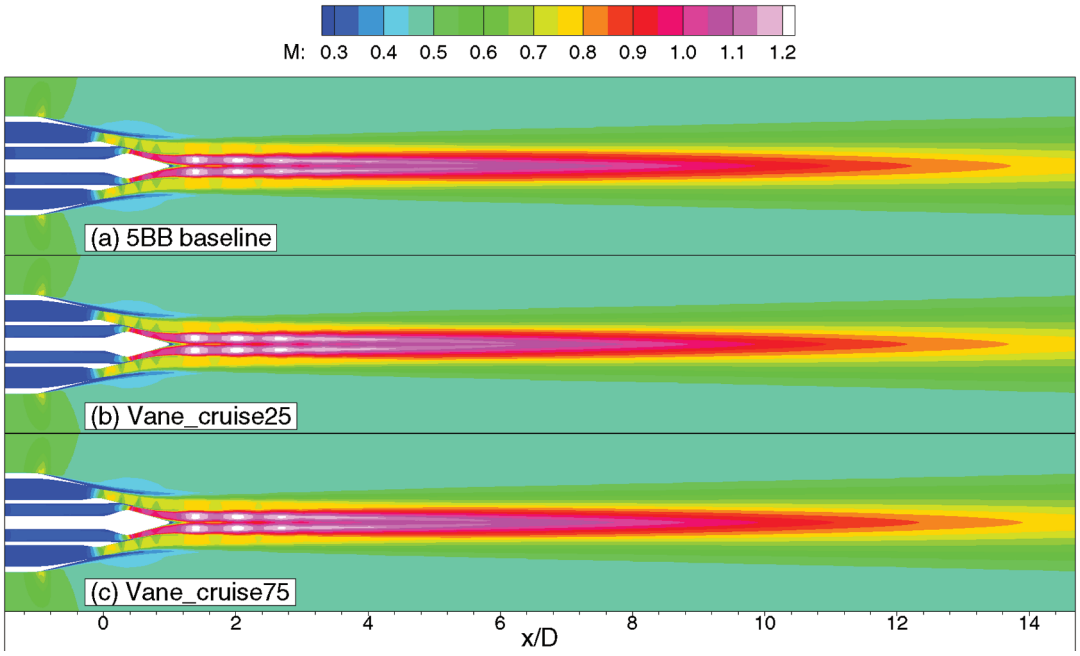

Fig. 20 Velocity contours on symmetry plane of vane nozzles and baseline at cruise flow conditions.

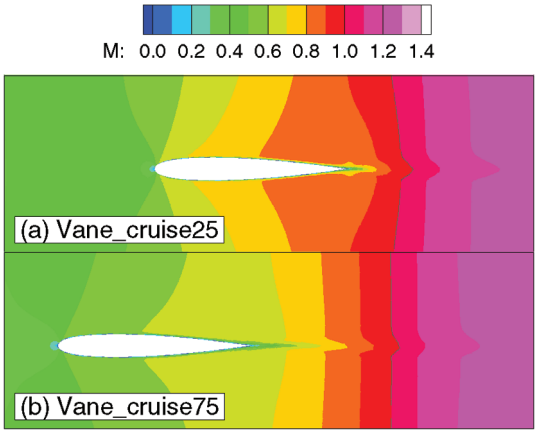

Fig. 21 Mach number contours at midspan of lower vane for vane offset-stream nozzles at cruise flow conditions.

quality [7]. This explains why there are blank, or white, areas around the jet plumes and even inside the jet plumes. Therefore, the CFD solutions are being compared only with the higher-quality PIV data. The CFD solution of the 5BB baseline nozzle showed excellent agreement with the PIV velocity data through most of the plume. The only exception is that the CFD solution prolonged the breakdown of the potential core in the region 5 to 7D downstream of the fan nozzle exit. This is not an isolated occurrence of this problem, but rather a known limitation of the RANS-based solutions for a number of turbulence models [14]. The CFD predictions of velocity for the S-duct and vane nozzles compared very well with the PIV data, matching in magnitude and structure. Contours of turbulence in the plume are compared between the CFD solutions and PIV data in Figs. 25–27. The CFD solutions did a good job of predicting the structure of the turbulence in the plume. The only major disagreement observed was that the CFD solutions did not predict the corners in the vane plume to be as sharp as that shown in the PIV data. In addition to prolonging the breakdown of the jet potential core, the CFD solutions predicted the peak levels of turbulence to be smaller than that observed in the PIV data. This has been found to be problematic for computational jet-noise-prediction codes [16], as jet noise is directly related to the turbulence.

The acoustics measurements reported by Henderson et al. [6] and Brown and Bridges [7] did show some reduction in jet noise for the offset-stream nozzles. However, the results were mixed. The offset-stream nozzles using vanes reduced low-frequency jet noise at certain observation angles. The offset-stream nozzle using the S-duct reduced noise at static freestream conditions, but increased noise at

Table 5 Mach number at vane leading-edge and training-edge locations in the baseline 5BB nozzle at cruise conditions

$(x/c)_{TE}$	M_{LE}	M_{TE}
$-\frac{1}{4}$	0.53	0.87
$-\frac{3}{4}$	0.44	0.66

$M_\infty = 0.20$ flight conditions. Yet, CFD simulations were still successful during the design and screening phases to predict the thrust performance and flowfield characteristics of the offset-stream nozzles. Using the knowledge gained from the experimental results, CFD could be used to further design and optimize offset-stream nozzles to produce a flowfield to reduce noise.

Conclusions

CFD simulations were performed on offset-fan-stream nozzles using S-ducts and vanes in preparation for experimental jet-noise and flow-measurement testing in the NASA GRC nozzle acoustic test rig. The offset-fan-stream nozzles were designed to reduce jet noise by redirecting the fan stream to the lower side of the nozzle to reduce the velocity gradient. Thirteen different offset-fan-stream-nozzle configurations were simulated: eight nozzles at takeoff conditions and five nozzles at cruise conditions.

At takeoff conditions, the S-duct and vane nozzles successfully directed the fan stream downward as intended. Turbulence levels on the lower side of the offset-fan-stream nozzles were greatly reduced, with peak values of turbulent kinetic energy being reduced by 10–11% over the associated baseline dual-stream nozzles. The nozzle thrust coefficient was computed from the CFD simulations and also showed that the offset-fan-stream nozzles performed relatively well compared with the baseline nozzles. There was less than 0.5% reduction in the thrust parameter at takeoff and less than 0.1% reduction in the thrust parameter at cruise.

The CFD calculations proved to be a vital part of the design phase of these offset-fan-stream nozzles. In CFD simulations of early vane-nozzle configurations, it was learned that vane angles of attack of 12 and 15 deg were too aggressive. The flow separated over these high-angle-of-attack vanes and significantly reduced thrust performance. For the S-duct nozzles, the CFD simulations showed that, contrary to the initial thought, a moderate amount of offset produced less turbulence on the lower side of the nozzle than did an aggressive amount of offset. Using CFD simulations during the design and screening phases of the offset-fan-stream program allowed the experimental phase to focus on nozzles that should both reduce noise and have good thrust performance.

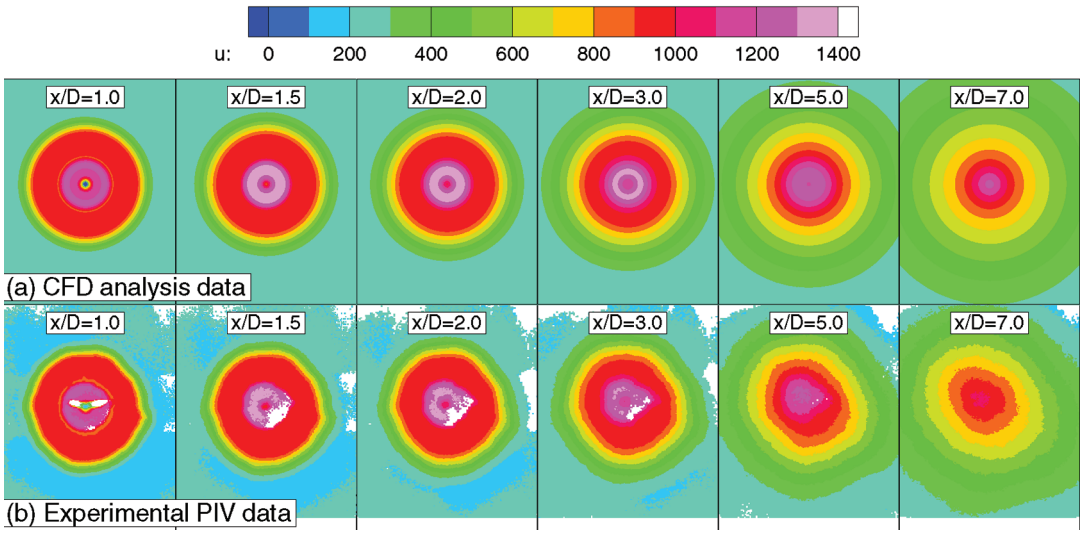

Fig. 22 Velocity contours of 5BB baseline nozzle at experimental flow conditions; $M_\infty = 0.20$.

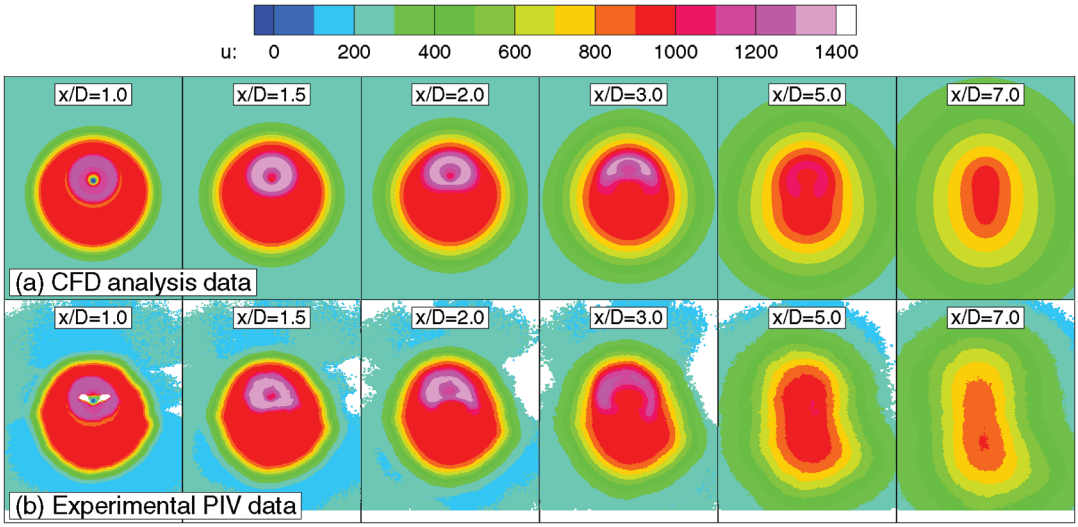

Fig. 23 Velocity contours of Sduct-5BB-45 offset-stream nozzle at experimental flow conditions; $M_\infty = 0.20$.

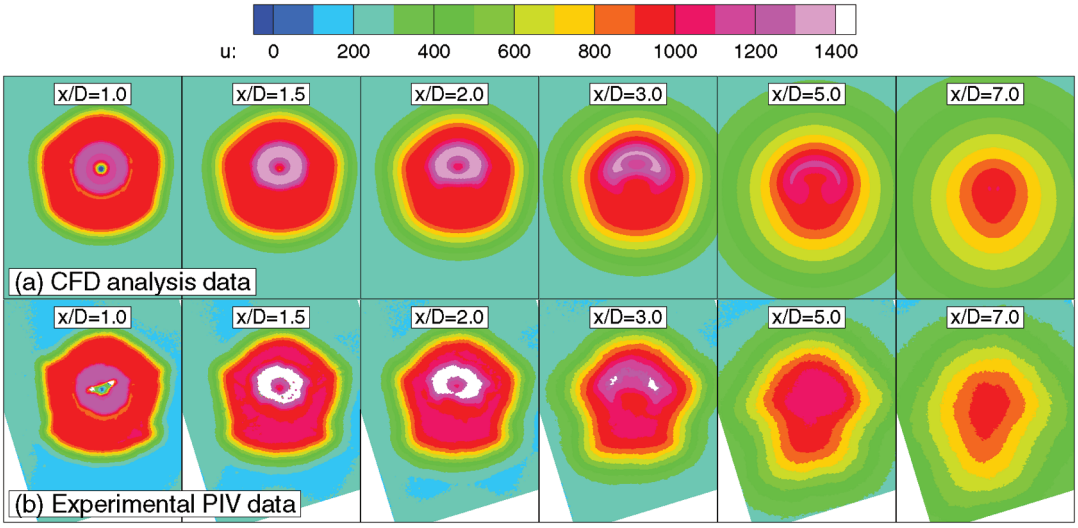

Fig. 24 Velocity contours of vane_E offset-stream nozzle at experimental flow conditions; $M_\infty = 0.20$.

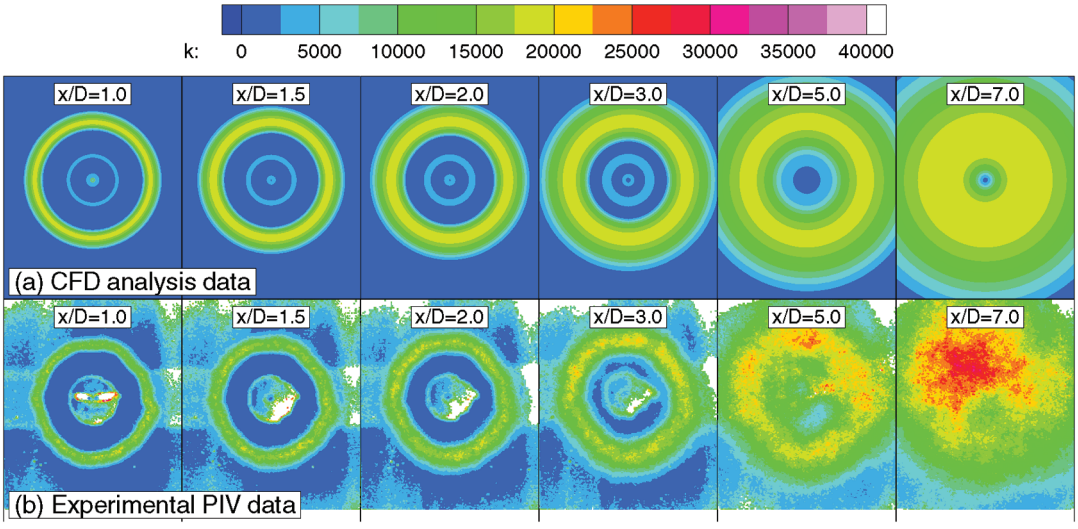

Fig. 25 Turbulence contours of 5BB baseline nozzle at takeoff flow conditions; $M_\infty = 0.20$. k in units of ft^2/s^2.

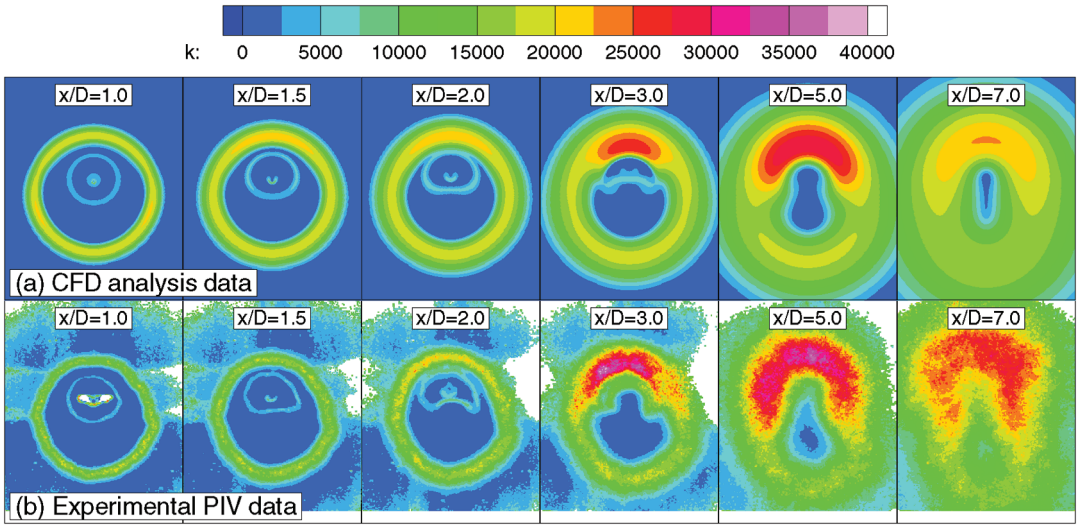

Fig. 26 Turbulence contours of Sduct-5BB-45 offset-stream nozzle at experimental flow conditions; $M_\infty = 0.20$. k in units of ft^2/s^2.

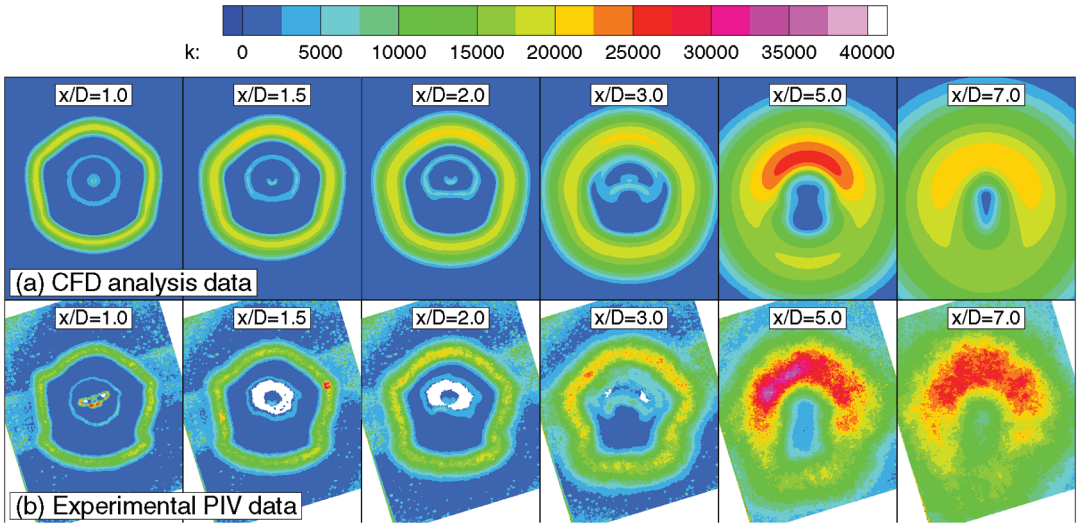

Fig. 27 Turbulence contours of vane_E offset-stream nozzle at experimental flow conditions; $M_\infty = 0.20$. k in units of ft^2/s^2.

The CFD results were compared with experimental particle image velocimetry (PIV) measurements at several axial planes downstream of the nozzle. The CFD predictions showed excellent agreement with the PIV velocity data. Although the CFD results did not capture the peak values of turbulent kinetic energy observed by the PIV measurements in the jet plume, the CFD results showed good agreement with the PIV data by predicting the trends of the turbulence in the plume.

Experimental acoustic measurements were taken for two of the offset-fan-stream nozzles presented in this report. Although reductions in jet noise were observed for offset-fan-stream nozzles using S-ducts and vanes, the results were mixed. From the understanding of offset-fan-stream nozzles gleaned from the experimental acoustic and flowfield measurements, CFD simulations could be successfully used to further design and optimize nozzles that effectively tailor the fan stream to reduce jet noise.

Acknowledgments

The authors wish to acknowledge the Quiet Aircraft Technology program for supporting this research effort. Additional gratitude is given to Nicholas Georgiadis, Jim DeBonis, Dennis Yoder, and Charlie Towne for their input and guidance and to James Bridges and Cliff Brown for providing the experimental flow data.

References

[1] Papamoschou, D., and Debiasi, M., "Conceptual Development of Quiet Turbofan Engines for Supersonic," *Journal of Propulsion and Power*, Vol. 19, No. 2, 2003, pp. 161–169. doi:10.2514/2.6103

[2] Papamoschou, D., "A New Method for Jet Noise Reduction in Turbofan Engines," *AIAA Journal*, Vol. 42, No. 11, 2004, pp. 2245–2253. doi:10.2514/1.4788

[3] Papamoschou, D., "Fan Flow Deflection in Simulated Turbofan Exhaust," *AIAA Journal*, Vol. 44, No. 12, 2006, pp. 3088–3097. doi:10.2514/1.22552

[4] Papamoschou, D., "Parametric Study of Fan Flow Deflectors for Jet Noise Suppression," AIAA Paper 2005-2890, May 2005.

[5] Zaman, K. B. M. Q., "Noise- and Flow-Field of Jets from an Eccentric Coannular Nozzle," AIAA Paper 2004-5, Jan. 2004.

[6] Henderson, B., Norum, T., and Bridges, J., "An MDOE Assessment of Nozzle Vanes for High Bypass Ratio Jet Noise Reduction," AIAA Paper 2006-2543, May 2006.

[7] Brown, C., and Bridges, J., "Offset Stream Technologies Test-Summary of Results," AIAA Paper 2007-3664, May 2007.

[8] DeBonis, J., "RANS Analyses of Turbofan Nozzles with Wedge Deflectors for Noise Reduction," AIAA Paper 2008-41, Jan. 2008.

[9] Janardan, B. A., Hoff, G. E., Barter, J. W., Martens, S., Gliebe, P. R., Mengle, V., and Dalton, W. N., "AST Critical Propulsion and Noise Reduction Technologies for Future Commercial Subsonic Engines:

Separate-Flow Exhaust System Noise Reduction Concept Evaluation," NASA CR-2000-210039, 2000.

[10] Abbot, I. H., and von Doenhoff, A. E., *Theory of Wing Sections: Including a Summary of Airfoil Data*, Dover, New York, 1959, pp. 321, 462–463.

[11] Bush, R., Power, G., and Towne, C., "WIND: The Production Flow Solver of the NPARC Alliance," AIAA Paper 1998-935, Jan. 1998.

[12] Nelson, C. C., and Power, G. D., "CHSSI Project CFD-7: The NPARC Alliance Flow Simulation System," AIAA Paper 2001-594, Jan. 2001.

[13] Georgiadis, N., and Papamoschou, D., "Computational Investigations of High-Speed Dual-Stream Jets," AIAA Paper 2003-3311, May 2003.

[14] Georgiadis, N. J., Rumsey, C. L., Yoder, D. A., and Zaman, K. B. M. Q., "Turbulence Model Effects on Calculation of Lobed Nozzle Flowfields," *Journal of Propulsion and Power*, Vol. 22, No. 3, 2006, pp. 567-575.
doi:10.2514/1.17160

[15] Menter, F. R., "Two-Equation Eddy Viscosity Turbulence Models for Engineering Applications," *AIAA Journal*, Vol. 32, No. 8, 1994, pp. 1598-1605.
doi:10.2514/3.12149

[16] Khavaran, A., Bridges, and Georgiadis, N., "Prediction of Turbulence-Generated Noise in Unheated Jets, Part 1: JeNo Technical Manual (Version 1.0)," NASA TM-2005-213827, 2005.

F. Liu
Associate Editor